Building and Environment 197 (2021) 107830

Contents lists available at ScienceDirect

Building and Environment

journal homepage: www.elsevier.com/locate/buildenv

Implementation of model predictive control in a large-sized, low-energy office building

Svenne Freund *, Gerhard Schmitz

Institute of Engineering Thermodynamics, Hamburg University of Technology, Denickestraße 17, 21073 Hamburg, Germany

ARTICLE INFO

Keywords:
Model predictive control
Field test
Optimization
Thermally activated building system (TABS)
Modelica

ABSTRACT

Modern and energy-optimized buildings often lack an intelligent and advanced control strategy. Instead, conventional rule-based control (RBC) strategies are still mainly used today, which do not exploit the full performance potential of these buildings. Model predictive control (MPC) has proven in simulation studies and pilot cases to be a promising approach to reduce the energy consumption of buildings, while improving occupants' comfort. However, there is still a lack of implementing MPC in real, large-scale and fully occupied buildings, to further prove this potential in real building operations. This paper describes the implementation and operation of MPC in a large-sized, low-energy office building. The MPC controller was implemented in a section of the building during a three-month test period from February to April 2020, controlling the supply temperature of heating circuits for thermally activated building systems (TABS). Its performance was compared to the default rule-based control which is active in the other building sections. This allows for a detailed evaluation of MPC versus RBC under identical environmental and operational conditions. The MPC controlled building section used 30 % less heating energy than RBC controlled building sections, while the existing high level of thermal comfort could be maintained. Especially in transition periods (i. e. interseasonal periods like late winter/early spring) , the MPC is superior to the conventional heating-curve based control strategy, with heating energy savings of 75 %.

1. Introduction

Against the background of the environmental impact of energy use, the depletion of primary energy resources and the associated economic consequences, considerable efforts are being made to realize environmentally-friendly and energy-efficient buildings. According to the European Commission, about 40% of the primary energy demand can be allocated to the building sector [1]. Thus, reducing the energy demand of buildings is a challenge of major importance to meet climate protection goals.

Especially in modern, energy-optimized and highly insulated buildings, the influence of the control strategy of the energy supply system on the overall energy-efficiency is often underestimated, as this is usually not considered during the design stage. Often simple, rule-based control (RBC) strategies are implemented in buildings, which are not or insufficiently adjusted to the underlying system [2]. Thus, the full potential of these buildings is not exploited. This is especially true for non-residential buildings such as large office buildings, which are equipped with complex hybrid energy supply systems and multiple heat distribution systems with different time constants, such as thermally activated building systems (TABS), floor heating, radiators and air-handling units (AHU) [3].

Advanced control strategies, like model predictive control (MPC) have been shown to be capable of improving the thermal comfort of occupants, while simultaneously reducing the energy demand of buildings in a range of 15% to 50% [4]. With the increase in performance and capacity of modern computers and the growing extensive use of measurement and monitoring systems, the investigation and implementation of advanced control strategies has gained increasing attention in recent years [5]. Furthermore, the upgrade and optimization of a building's control systems is comparatively cost-effective compared to the refurbishment of buildings.

However, the implementation of MPC is in practice still far from trivial [6]. This is due to the fact that each building is unique with regard to its construction, its subsystems and its hardware and software solutions, thus requiring a tailored design of advanced, model-based control strategies. While many studies have analyzed the potential of MPC based on simulations, the number of practical implementations of MPC strategies is still limited, especially for occupied and fully operated large-sized buildings [7]. One of the first experimental analyses of MPC was reported in [8,9] where a two-month experiment was performed on a university building in Prague, Czech Republic. The study focused

* Corresponding author.
E-mail addresses: svenne.freund@tuhh.de (S. Freund), schmitz@tuhh.de (G. Schmitz).

https://doi.org/10.1016/j.buildenv.2021.107830
Received 14 December 2020; Received in revised form 19 March 2021; Accepted 20 March 2021
Available online 27 March 2021

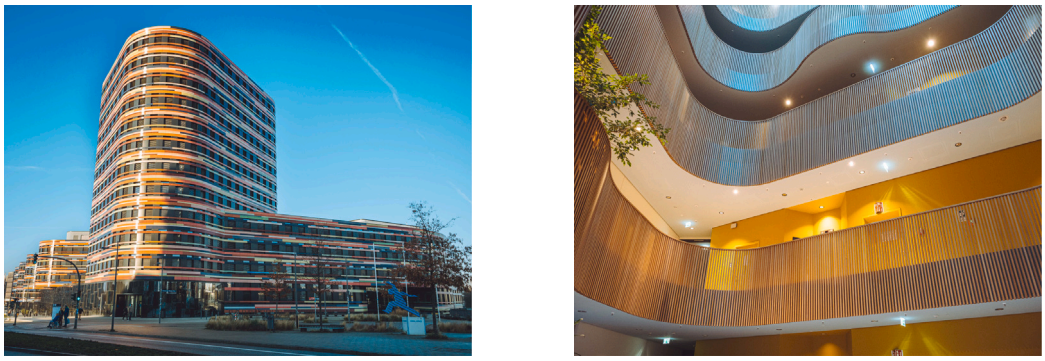

Fig. 1. Exterior (left) and interior (right) view of the office building.

mainly on energy savings and the range of saving potential was reported as 15% to 28% during the heating season, depending mainly on insulation level and outside temperature. A linear state-space model identified from measurement data was used to describe the building's thermal behavior and the cost function was formulated as a quadratic programming (QP) problem. In [10] the successful implementation of MPC to control TABS, AHU and blinds in a modern Swiss office building were demonstrated with very satisfying results in terms of thermal comfort. Similarly, a case study using a gray-box model of a medium-sized office building in Brussels, Belgium, obtained 20% to 30% energy savings during the heating season [11]. A very recent field test demonstration of MPC in a GEOTABS office building, quite similar to the building investigated in this paper, is given in [12]. The linear state space controller model was derived from a detailed white-box model and the arising optimization problem was split into a QP and a smaller non-linear program (NLP). Real operation during the transient season resulted in energy savings of 53.5% and thermal comfort improved by 36.9% compared to RBC. The application of MPC is by far not limited to the control of heating systems. Other applications of MPC are smart-grid integration [13] and demand-side management [14], the control of cooling systems for buildings [15], or data centers [16] and the control of dynamic facades [17].

This paper presents a three-month field test demonstration of MPC in a modern large-sized, energy-efficient office building in Hamburg, Germany. A gray-box model approach in combination with a dedicated parameter identification method is chosen to describe the dynamic thermal behavior of building zones. These gray-box models are implemented in the equation-based modeling language Modelica [18] which allows easy formulation and efficient solution of non-linear optimization problems [19]. The Modelica models identified are used directly by the controller developed, without any further post-processing or linearization steps, resulting in a non-linear optimization problem which is still small enough to be integrated into a real-time control application. The unique experimental setup allows a detailed comparison of MPC and RBC controlled building sections under identical environmental and operational conditions, with regard to heating energy demand and thermal comfort. Previous investigations of the building revealed an anti-correlation between the outside air temperature and indoor air temperature, i. e. that the building tends to overheat on cold, clear-sky winter days, which indicates a non-optimal setting of the control strategy. The MPC approach is promising for eliminating these problems. The building investigated was already planned and built as a highly energy efficient and sustainable building. Therefore, a question that this paper tries to answer is what contribution building control, i. e. pure software measures, make to the building energy efficiency.

The paper is structured as follows. The office building investigated is presented in Section 2. The development of the zone model used by the controller is based on a gray-box modeling approach, which is described in Section 3. In Section 4, the MPC algorithm is formulated and details of the communication infrastructure are provided. The experimental results of the MPC operation are presented in Section 5. Finally, Section 6 presents the paper's conclusions.

Table 1
General geometrical and thermophysical properties of office spaces.

Description	Unit	Value
Width	m	2.5
Clear height	m	2.9
Floor area	m^2	10 to 13
External wall area	m^2	2.63
U-value glazing	$W\,m^{-2}\,K^{-1}$	0.7
U-value facade	$W\,m^{-2}\,K^{-1}$	0.9

2. Office building

The office building investigated, shown in Fig. 1, is the headquarters of the two local ministries for energy and environment and urban development and housing in Hamburg, Germany. With a net floor space of 46 500 m^2, the building provides space for around 1500 workplaces in 1250 offices. It consists of two wings with a total of seven 5-story low-rise buildings (referred to as Buildings A-D and F-H) and a central 13-story high-rise building (referred to as Building E), see Fig. 2. The building was constructed in 2013 as part of the International Building Exhibition within the research initiative Energy-Optimized Building (EnOB). With an annual primary energy demand of less than 70 kWh/m^2 and a maximum heating energy demand of 15 kWh_{th}/m^2 as target values, the building can be classified as very energy efficient and sustainable.

2.1. Standard office layout

The majority of office spaces inside the building are used as single offices with rectangular floor space, see Fig. 2. Additionally, there are offices with convex or concave outer façades in the curved building parts, which are often designed as double offices. The general geometrical and thermophysical properties of typical office spaces are summarized in Table 1. Each office has manually openable windows and weather-proofed ventilation flaps. The windows are equipped with triple-glazing and automated external shading devices. The building's facade is realized as a unitized curtain wall with ceramic panels mounted on the outside. Office spaces are heated by thermally activated building systems in the form of thermoactive ceilings (TAC), i. e. by thermally activating the concrete-core of the slabs. During winter, mechanical ventilation with preheated air is used to supply fresh air. In summer mode, the building's office areas are passively cooled by the TAC and mechanical ventilation is replaced by manual ventilation using the ventilation flaps.

2.2. Heating system

The schematic layout of the energy supply system is shown in Fig. 3. The building's heating system is mainly based on the use of shallow geothermal energy in combination with two electrically driven heat

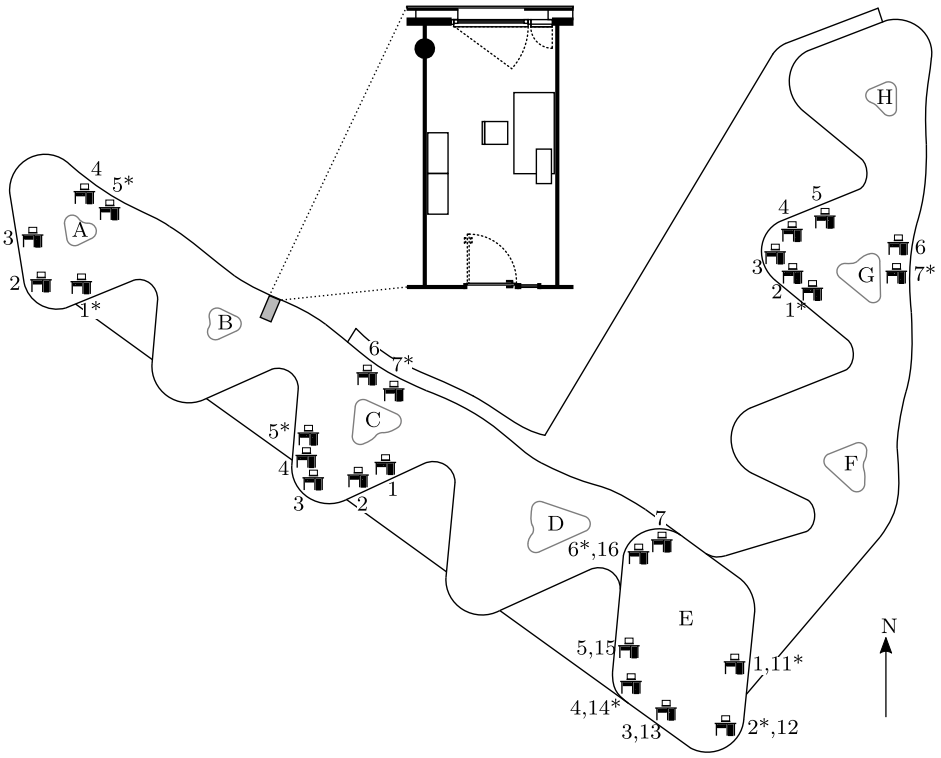

Fig. 2. Simplified floor plan of the building investigated with distribution and orientation of reference office spaces. Reference office spaces marked with "*" are extended reference office spaces.

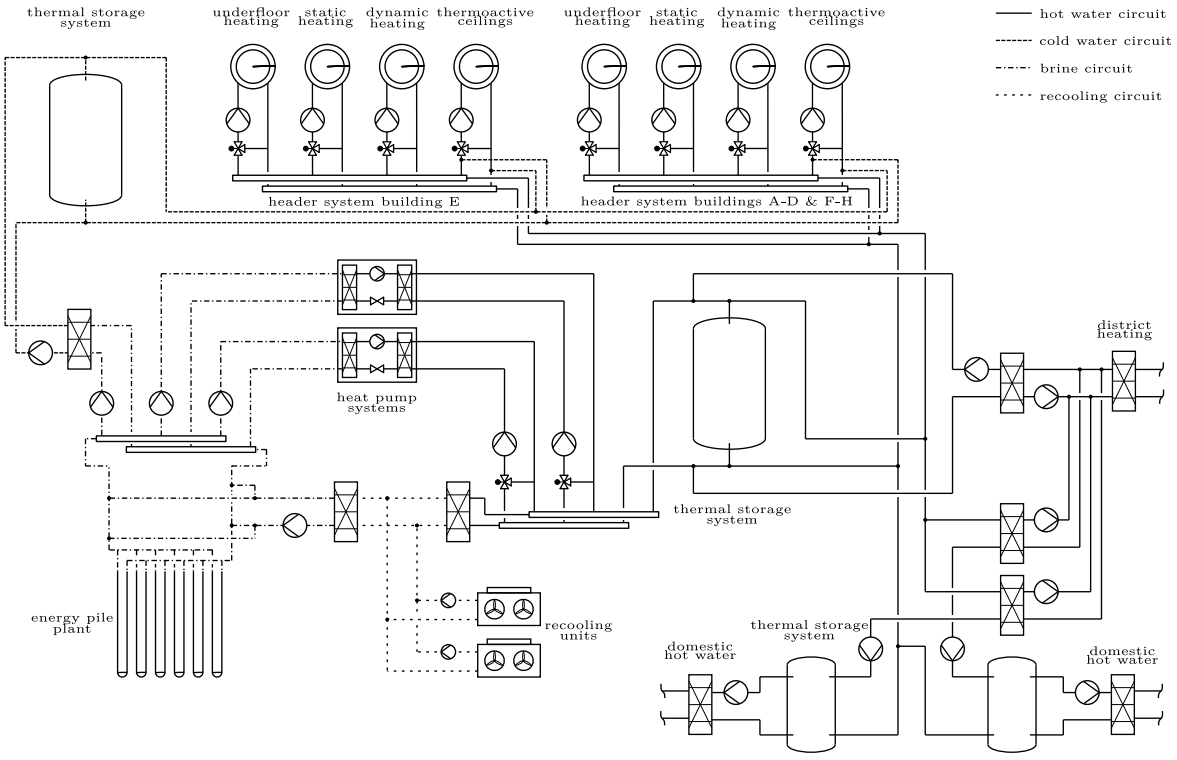

Fig. 3. System layout of thermal energy supply.

pumps, each with a nominal thermal power output of 264 kW_{th}. For domestic hot water supply and for peak load coverage, there is an additional connection to a district heating network with a nominal thermal power output of 750 kW_{th}. Both systems feed a central hot water storage with a capacity of 5 m^3. As described above, the main building areas are heated by thermoactive ceilings. Other functional areas of the building, like corridors and basement areas, are heated using underfloor heating or static heating (i. e. radiators and convectors). The heating circuit

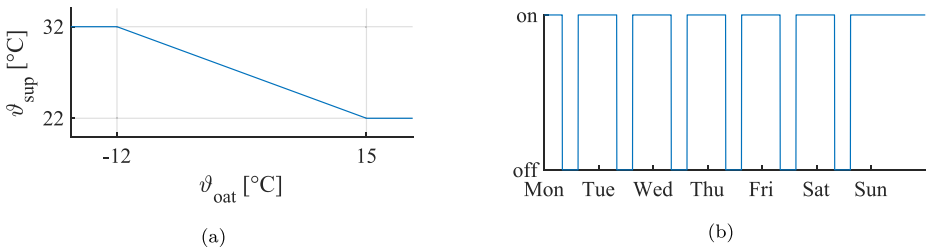

Fig. 4. Heating curve (a) and heating schedule (b) for the supply water temperature of the TAC heating circuits.

called "dynamic heating", see Fig. 3, is used to reheat process air to a desired supply air temperature within the air handling units. As such, this heating circuit serves actually not for heating purposes, but rather for mechanical ventilation. In summer mode, the geothermal system is used as a heat sink for the TAC. The other heating circuits are not active during summer mode.

2.3. Control system

This study focuses on controlling the TAC heating circuits using MPC. The control of the other system components (e. g. heat pump, district heating, domestic hot water) and heating circuits (underfloor heating, static heating, dynamic heating) remains unchanged and is therefore not described in detail here.

Each of the eight building sections has two TAC heating circuits differentiated by orientation (south/north and south-west/north-west respectively) resulting in 16 different control loops. Originally, each of these heating circuits is controlled by a rule-based controller (RBC). The RBC uses a heating curve, see Fig. 4a, for the supply water temperature set points in combination with a simple heating schedule shown in Fig. 4b. The heating curve is a linear function of the current on-site measured outside air temperature (OAT). The heating schedule defines the period where heating can be activated, i. e. by activating the feed pumps. An internal logic in the building management system (BMS) calculates the optimal start and stop time based on the moving average of the OAT. PI controllers then modulate the opening of the three-way valves to control the supply temperature in each heating circuit to the given set point. Therefore, the current RBC can be considered as an open-loop controller, since it does not integrate feedback of zone temperatures as control variables.

The other heating circuits (underfloor, static and dynamic heating) are controlled similarly, but using different heating curves and schedules. Switching between winter and summer mode is done automatically by the BMS using the moving average OAT of the last 36 h.

2.4. Monitoring system

The building was investigated and supervised in a scientific monitoring project which started in July 2014. The aim of this monitoring was to examine the energy demand targets and to consistently optimize the building operation with respect to user comfort and operating costs. Results of the monitoring project can be found in [20]. The monitoring system comprises an extensive network of more than 1100 sensors consisting of various energy meters, flow meters and temperature sensors, to measure and record the relevant parameters within the different subsystems with a sample rate of 1 min. To additionally analyze and evaluate the user comfort, 32 *reference office spaces* were equipped with sensors for air temperature, relative humidity, presence and window handling. The location of these reference office spaces is shown in Fig. 2. Reference office spaces marked with "*" are extended reference offices where sensors for radiation temperature, surface temperature of the ceiling and CO_2 concentration are installed additionally.

3. Development of building model

The core of MPC consists of one or more dynamic models that can describe the thermal behavior of the building or particular building zones. The accuracy of these controller models is crucial for the overall performance of the MPC controller [21]. These models must be reasonably fast in terms of their simulation time, since they are used in an online optimization problem solved almost in real-time. This section describes the structure of the controller model used.

3.1. Gray-box model

A gray-box modeling approach is chosen to represent the thermal behavior of building zones. This approach is motivated by several successful applications of gray-box models for predictive control strategies. Fig. 5c shows the RC network representation of the model used.

A building zone is represented by a single reference office space, see Fig. 5a. Later, the controller incorporates several zone models located on the 4th floor of a building section (see Fig. 2) to control the TAC heating circuit of the entire building section. Supported by measurements, it is therefore assumed that the reference offices are representative of all other offices. Due to the system design, individual control of floors or even offices is not possible, i. e. it is assumed that if thermal comfort conditions are met in the reference office spaces, this holds true for all other office spaces too.

The gray-box model consists of seven resistances and four capacities (R7C4 model). The four state variables T_W (external wall temperature), T_{Air} (indoor air temperature), T_{Int} (temperature of internal masses) and T_{TAC} (TAC core temperature) correspond to the four thermal capacities C_W, C_{Air}, C_{Int} and C_{TAC}. The thermoactive ceiling (see Fig. 5b) consists of 30 cm reinforced concrete with an above lying cavity floor. The PEX pipes are located close to the lower surface to optimize the heat flow to the room below. Based on the EMPA model [22], a simplified model for the TAC is used consisting of two resistances R_{TAC1} and R_{TAC2}. By assuming equal room temperatures below and above the thermoactive ceiling, the two heat flow paths to respectively the room above and below the ceiling can be transformed into a single heat flow path, resulting in a R2C1 TAC model [23]. By using a semi-physical and data-driven modeling approach, a potential heat input through the floor can be included within this very simple TAC model. However, due to construction of the ceiling/floor and supported by thermographic measurements, a significant heat input through the floor is not to be expected. The external wall is modeled with two resistances for the envelop (R_{W1} and R_{W2}) and one resistance for the glazing R_G. Mechanical ventilation is represented with one resistance R_{MV}. The resistance R_{Int} describes the heat exchange between the air volume and the internal masses. Heat exchange between adjacent zones is neglected, since it is assumed that there are no large temperature differences between the zones.

In total, the model has five inputs: outside air temperature T_A, supply temperature of the corresponding TAC heating circuit $T_{Sup,TAC}$, supply temperature of mechanical ventilation $T_{Sup,MV}$, global solar radiation on the corresponding facade orientation and occupancy state. For the heat exchange between the building and the environment, a

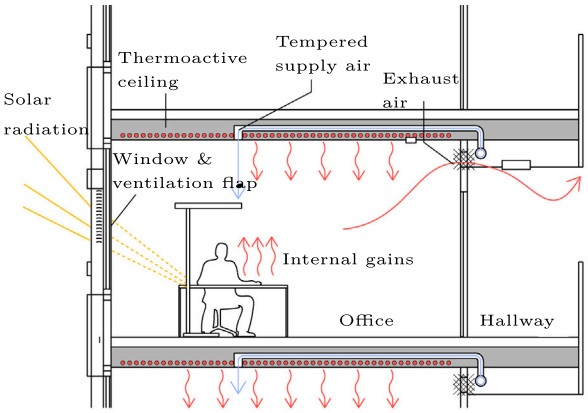

(a) Schematic of standard single office.

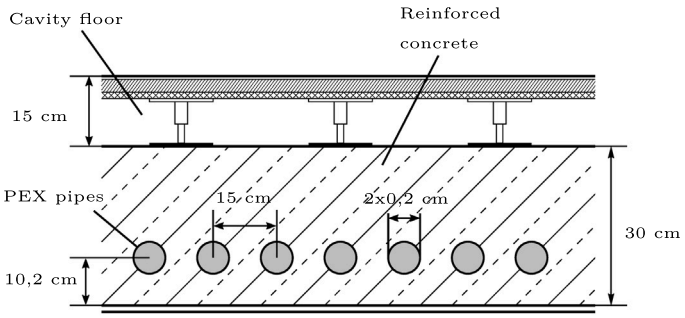

(b) Schematic of thermoactive ceiling.

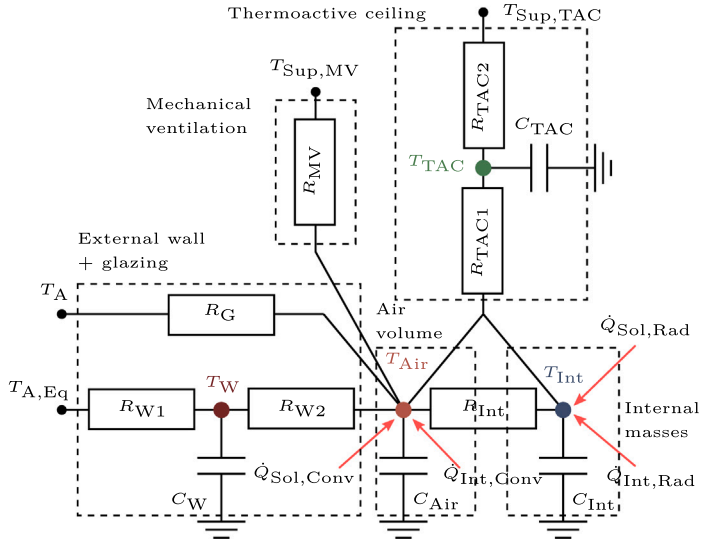

(c) RC network representation of gray-box zone model.

Fig. 5. Schematic of a standard single office (a), schematic of the thermoactive ceiling (b) and thermal network representation of the gray-box model used consisting of thermal resistances and capacities (c).

simple approach is chosen based on VDI 6007 [24] using the equivalent outdoor air temperature $T_{A,Eq}$. Internal heat gains by persons, lighting or other equipment $\dot{Q}_{Int}$ are calculated using the measured occupancy state multiplied by a constant factor. Internal and external heat gains are split into convective parts acting on the air volume and radiative parts acting on the internal masses.

A dedicated parameter method is used to identify the values of the free model parameters using measured input and output data from previous years of operation. More information about the model and the identification method can be found in [25] and [26]. The gray-box model shown in Fig. 5c is implemented in the equation-based, object-oriented modeling language Modelica [18]. An API to MATLAB® is developed which enables access to parameters and states.

4. Model predictive control

This section describes the formulation of the MPC algorithm, which mainly consists of the cost function and the disturbance forecast. Moreover, the architecture of the communication infrastructure for the implementation in the real building is presented.

4.1. Cost function formulation

The objective of MPC is to minimize the heating energy demand and thermal discomfort of the building. Therefore, the following cost function of the constrained nonlinear optimization problem is to be minimized:

$$\arg\min_{u(t)} \left\{ \alpha \cdot J_e + \beta \cdot J_{dc} \right\} \tag{1a}$$

subject to:

$$F(\dot{x}_i(t), x_i(t), y_i(t), u(t), d_i(t), p_i) = 0 \tag{1b}$$

$$u_{min} \leq u(t) \leq u_{max} \tag{1c}$$

$$\Delta u(t) \leq \Delta u_{max} \tag{1d}$$

$$x_0 = \tilde{x}(t) \tag{1e}$$

$$J_e = \sum_i \int_0^{t_c} \dot{Q}_{zone,i}(t)\mathrm{d}t \tag{1f}$$

$$J_{dc} = \sum_i \int_0^{t_c} f_{dc,i}(t) \cdot f_{occ}(t)\mathrm{d}t \tag{1g}$$

where x_i, y_i, u, d_i and p_i represent the states, outputs, inputs, disturbances and parameters for each zone $i = (1, \ldots, n_{zone})$ respectively.

Table 2
Main parameters of MPC problem.

Symbol	Description	Value
$u_{\min}$	Lower bound of TAC supply temperature	22 °C
$u_{\max}$	Upper bound of TAC supply temperature	32 °C
$\Delta u_{\max}$	Maximum rate of change of TAC supply temperature	4 K/h
$T_{\text{zone,min}}$	Lower zone temperature bound	21.5 °C
$T_{\text{zone,max}}$	Upper zone temperature bound	23.5 °C
$t_{\text{occ,start}}$	Occupancy start time	6:00 AM
$t_{\text{occ,end}}$	Occupancy end time	6:00 PM

The predicted model response of each zone is obtained from (1b) which is given in the implicit form of a differential–algebraic system of equations (DAE system) and is solved directly in Dymola. For each zone, a separate R7C4 model is used. The number of zones incorporated by the controller corresponds to the number of reference office spaces in the MPC controlled building section, see Fig. 2. The outputs of each zone model $y_i = (T_{\text{zone},i}, \dot{Q}_{\text{zone},i})$ are the zone temperature and supplied heat flow. The control input u (supply temperature set points of the corresponding TAC heating circuit) is constrained by the lower and upper limits $u_{\min}$ and $u_{\max}$ and by a maximum rate of change $\Delta u_{\max}$. The disturbances d_i comprise the weather forecast, the expected occupancy profile and the schedule for mechanical ventilation. The energy cost function J_e is the sum of heat supply for each zone integrated over the control horizon t_c. Costs for discomfort are obtained from (1g) where $f_{\text{dc},i}$ is the penalty function for violating the comfort range defined as

$$f_{\text{dc},i}(t) = \begin{cases} \gamma \cdot |(T_{\text{zone},i} - T_{\text{zone,min}})| & \text{for } T_{\text{zone},i} < T_{\text{zone,min}} \\ \gamma \cdot |(T_{\text{zone},i} - T_{\text{zone,max}})| & \text{for } T_{\text{zone},i} > T_{\text{zone,max}} \\ 0 & \text{otherwise} \end{cases} \tag{2}$$

with γ as penalty factor and f_{occ} incorporates the occupancy schedule as

$$f_{\text{occ}}(t) = \begin{cases} 1 & \text{for } t_{\text{occ,start}} \le t \le t_{\text{occ,end}} \\ 0 & \text{otherwise.} \end{cases} \tag{3}$$

For the given initial conditions (1e) and disturbances, the optimization computes the optimal control trajectory $u^*(t)$ with respect to the objection function (1a) and constraints. In (1a), α and β are weighting factors for energy and discomfort cost respectively.

The main parameters of the MPC problem are shown in Table 2. As the MPC controller is expected to control the zone temperatures close to the lower bound, the zone temperature bounds are chosen within a narrow range of 21.5 °C to 22.5 °C. The zone temperature constraints are only enforced during the expected occupancy time (6:00 AM to 6:00 PM). During non-occupancy time, the temperature is free-floating. The described MPC algorithm runs with a sample rate of 30 min and a prediction horizon of 48 h.

4.2. Disturbance forecast

The internal gains are determined by an occupancy profile which is based on the measured electricity consumption of office lighting using data from 2015 to 2019. The actual heating gains of each zone are obtained by multiplying the profile with a constant factor $\dot{Q}_{\text{occ}}$ which is determined in the identification process.

Mechanical ventilation is incorporated by a simple schedule (switch-on time: 7:30 AM, switch-off time: 5:30 PM) and a constant supply air temperature of 22 °C.

The weather forecast is based on the MOSMIX forecast of the German Weather Service [27] which is provided with a time step of one hour and a maximum forecasting time of 10 days. An API automatically downloads and post-processes the latest data of the station closest to the building such that it can be used as an input for the Modelica model.

4.3. Communication infrastructure

Fig. 6 demonstrates the technical scheme of the MPC operation in the building. MPC is designed as a high-level controller so that changes and interventions in the existing BMS are kept to a minimum. Trend 963 Supervisor by Honeywell [28] is used as the BMS. Communication between the BMS and the field automation level is carried out via a LON Network. The entire MPC program is implemented in MATLAB® and runs on a separate industry PC which was previously mainly used for monitoring. Exchanging measurements and set points between the high-level controller and the BMS is realized via OPC standard embedding a Trend OPC server and MATLAB® as a client using MATLAB® OPC Toolbox™ [29].

The main MPC algorithm is executed every 30 minutes via task scheduler. At the beginning, the latest weather forecast is downloaded and the current relevant measurements are gathered. An Unscented Kalman filter (UKF) updates the current state estimates of the zone models using the latest measured zone temperatures. The MATLAB® built-in solver `fmincon` is used to solve the optimization problem. The optimized set points for the next 48 h are then read by set point generator which runs with a sampling time of 1 min via MATLAB® timer and communicates the current set point value to the BMS via OPC.

By using Dymola and MATLAB®, the advantages out of both worlds are combined. Dymola takes care of modeling and solving the DAE system, while the powerful MATLAB® environment is used to set up the MPC algorithm, including solving the optimization problem and communicating with other systems. However, there are tools, such as OPTIMICA [30] or the Dymola Optimization Library [31], for solving optimal control problems in Modelica directly which have not been investigated here.

To ensure stable operations, a dedicated error handling and fallback strategy is implemented. In case of an error (e. g. communication error, failed download of weather forecast) the values from the previous time step are recovered and an email notification is generated. If the error occurs in more than three execution steps, a fallback strategy is triggered and the operation reverts to the original RBC strategy. However, no critical errors occurred during the three-month test period, so the MPC operation continuously ran without interruption.

5. Experimental results

The proposed MPC controller was implemented in the low-rise building section G (see Fig. 2) and therefore substituted the RBC of the two existing TAC heating circuits in this building section. Seven different gray-box models where used as controller models, corresponding to the seven existing reference offices spaces. The control of the other existing heating circuits for static heating (i. e. radiators in the basement area) and underfloor heating for corridors are unchanged and therefore are not part of this evaluation as they only play a very minor role to the building's heat input. Building G comprises 174 offices over a floor area of 2270 m^2. The experiment was conducted from February 1 to April 30, 2020, in full building operation. The other building sections remained in RBC operation. This unique experimental setup allows a direct and detailed comparison of the performance of MPC and RBC in similar building sections and under identical operating conditions. The following evaluation is subdivided into two parts. First, the performance of MPC with regard to the heating energy demand is analyzed. Thereafter, the thermal comfort is assessed on the basis of the existing reference office spaces, and a comparison is made between the two control strategies.

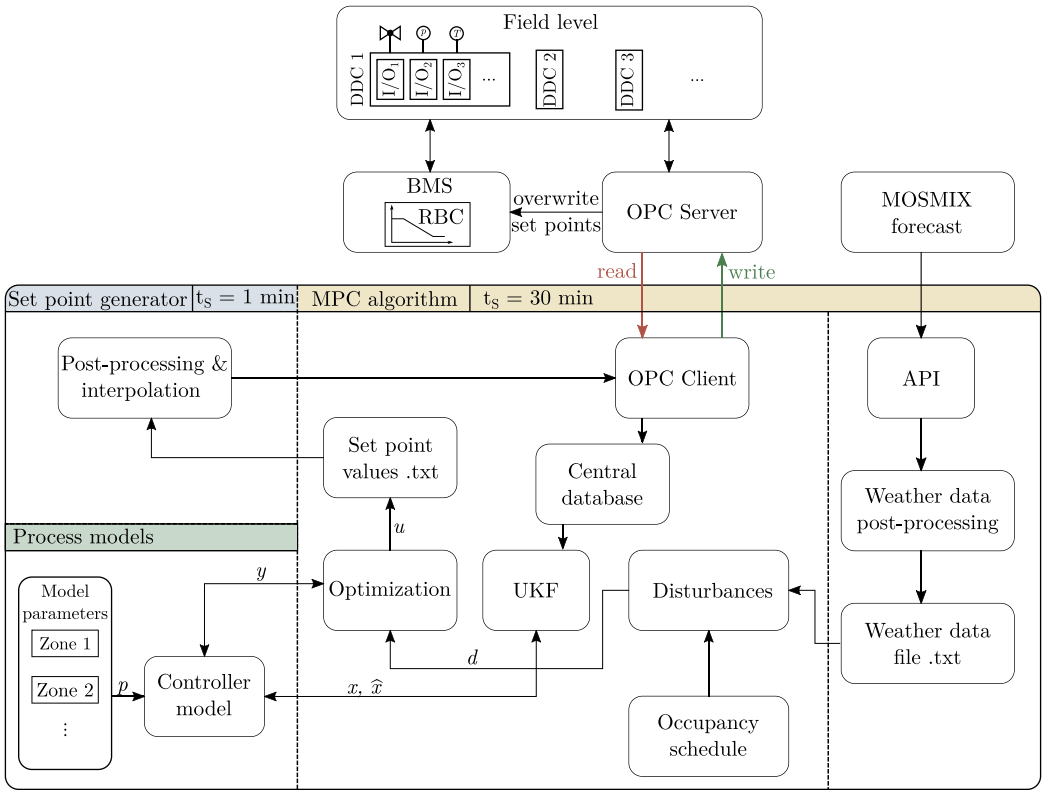

Fig. 6. Technical scheme of the high-level MPC controller.

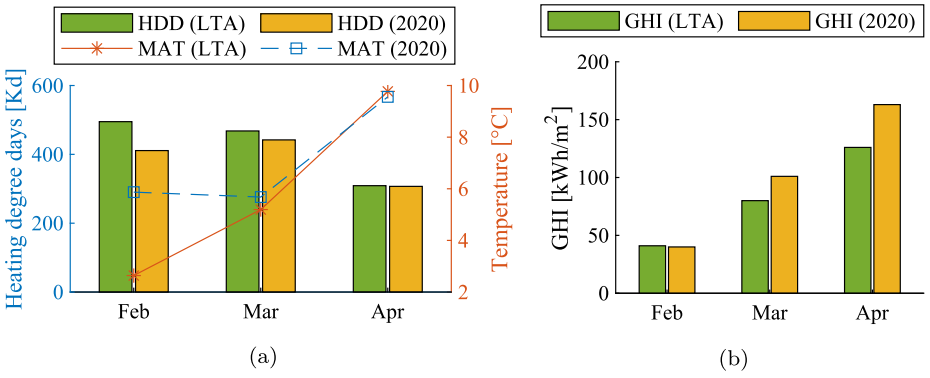

Fig. 7. Climate conditions for the period investigated. (a) heating degree days (HDD) and monthly average outside air temperature (MAT). (b) monthly sum of global horizontal irradiance (GHI). LTA is the long-term average (2000–2019).

5.1. Heating energy

To characterize the weather impact on the building's heating energy demand (HED), the heating degree days (HDD), the monthly average outside air temperature (MAT) and the monthly global horizontal irradiance (GHI) for the three months of evaluation are shown in Fig. 7. The data for the corresponding location is provided by the German Weather Service [32].

Regarding the outside air temperature, February 2020 was distinctively warmer while March and April can be described as average compared to the long-term average from 2000 to 2019. Accordingly, the HDD in February is 17% lower than the average. The monthly sum of global solar irradiance is more than 25% higher in March and April 2020 compared to the long-term average (LTA). In summary, the three-month evaluation period can be characterized as slightly warmer and significantly sunnier than average.

Fig. 8 shows the monthly heating energy demand in the period investigated and the average monthly heating energy demand of the previous years (2015–2019). As described previously, only the heating energy output of the TAC heating circuit is evaluated here. All heating energy demands are outdoor-temperature corrected according to VDI 3807 [33] using the HDD given in Fig. 7 and related to the respective heated floor area. The reference heating energy demand shown (referred to as Ref. in Fig. 8) is the average heating energy demand of the six low-rise building sections, except Building G. The high-rise building section E is omitted from this analysis, since the system's operating conditions differ significantly from the low-rise buildings. All heating energy demands are measured with a heat meter with a measurement uncertainty of ±6% of reading.

As shown in Fig. 8, the average heating energy demand of the RBC operated low-rise buildings in February and March 2020 corresponds very well to the five-year average from 2015 to 2019. In April 2020, the HED is 31% lower compared to the previous five years. Furthermore, the figure shows that the HED of the MPC operated Building G in 2020 was considerably reduced in all three months. To increase the

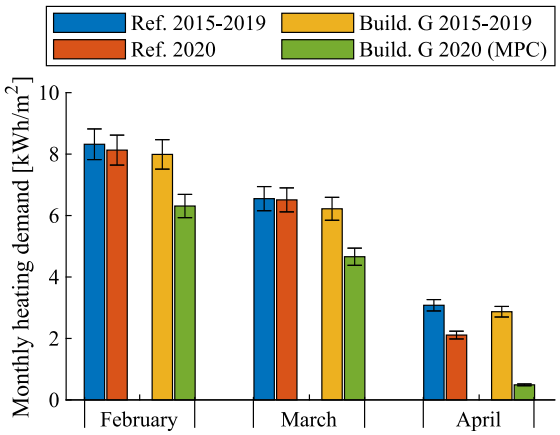

Fig. 8. Heating energy demand in the investigation period. The reference heating energy demand (Ref.) is the average heating demand of the low-rise buildings, except Building G.

Table 3
Heating energy demand and savings of Building G.

Quantitative indicators	February	March	April
Average heating energy demand (2015–2019, RBC) in kWh/m²	7.99	6.22	2.87
Corrected heating energy demand (2020, MPC) in kWh/m²	6.46	4.69	0.74
Absolute energy savings in kWh	3480	3476	4895
Relative energy savings in %	19.2	24.6	75.2

fairness of the comparison, the HED of Building G in 2020 is corrected by the ratio of the reference HED in 2020 to the five-year average of the reference HED. This correction takes into account that there are weather-independent effects that influence the heating energy demand, like changes in building operation or the influence of users.

Table 3 summarizes the HED of Building G and gives the absolute and relative energy savings per month. In the three months of investigation, MPC uses 11 784 kWh less heating energy than RBC, which corresponds to a relative saving of 30%. Especially in April, the MPC strategy is superior to the current RBC with the highest absolute and relative energy saving. The reasons for this can be found in the prevailing weather conditions. As described above, April 2020 was exceptionally sunny and characterized by a high difference between the minimum and maximum MAT, see Fig. 7. The RBC implemented generates the supply temperature set point based on the relatively cold outside air temperature mainly during night hours, resulting in high set point values, see Fig. 9. The MPC controller, on the other hand, "knows" about relatively high daytime air temperature and the high solar irradiation of the upcoming day, which leads to anticipatory behavior with low set point values and heating activity respectively. In addition, the MPC incorporates the feedback from zone temperature measurements and thus ensures that the heat losses during the night do not lead to a violation of the comfort zone.

A comparison of the supply temperature set points generated by RBC and MPC, shown in Fig. 9, reveals that MPC often uses higher maximum set points but shorter heating periods. For the very slow-reacting thermoactive ceilings, this is a favorable operating mode since it supports the charging/discharging behavior. RBC, on the other, hand uses a more continuous charging at moderate supply temperatures. In addition, Fig. 10 shows a week's zoom on the first week of March (2 to 8 March) of the supply temperatures including active periods of heating (i. e. where the feed pumps are activated) and the mean zone temperatures of the reference office spaces (see Fig. 2) with standard deviation. The figure reveals some basic features of the MPC strategy that also can be applied to other time periods.

As mentioned before, MPC results in shorter, but more pronounced heating periods with temporarily higher supply temperatures than given by the heating curve used by RBC. The basic temperature level of the providing heating system (i. e. secondary side of heat pumps, thermal storage system, cf. Fig. 3) is in a range of 40 to 50 °C, so that these higher supply temperatures do not increase the overall system's effort or operating costs. It is also worth noting that unlike RBC, the MPC controller never activates heating on Fridays. Due to the underlying occupancy schedule, no occupancy is scheduled in a 48-hour prediction horizon and thus no zone temperature control is needed. As a result, zone temperatures are free-floating on Friday and Saturday and a distinguished temperature drop can be identified. With RBC, the zone temperature on weekends is almost constantly at the same level as on weekdays. MPC starts heating around Saturday evening to meet the desired comfort range on Monday morning. In this case, however, a longer period of heating is required compared to the RBC strategy.

It is important to note that the improvements in terms of the HED may be partly attributed to exceptional weather conditions during March and April. A longer test period covering a complete heating season is planned. Furthermore, parts of the period investigated were characterized by the restrictions on public life due to the COVID-19 pandemic. These restrictions definitely had an influence on building operation and performance but it is very difficult to quantify these influences. For example, the building's overall occupancy rate was low due to the increasing number of employees working from home. Nevertheless, the results are very encouraging towards an extended investigation of the MPC performance in this building.

5.2. Thermal comfort

In order to assess the thermal comfort, the time-integrated violation of the comfort bounds measured in kelvin hours (Kh) is used. The comfort range is set to 20 °C to 24°C which corresponds to the category II defined in DIN EN 15251 [34]. Violation of comfort bounds is only counted during working hours. The following investigation of thermal comfort only includes the reference office spaces in the low-rise building sections. A comparison between the MPC operated Building G (seven reference zones) and the RBC operated Buildings A and C (five and seven reference zones respectively) is performed.

Fig. 11a depicts the room temperatures of the seven reference zones in Building G during the three-month investigation period. Fig. 11b shows the daily average thermal comfort violation per zone in Buildings A, C and G. As can be seen, the room temperatures are kept within the comfort range most of the time during February and the first three weeks of March. The violation of the lower comfort bound of 0.11 Kh/d in February is solely due to opening windows or ventilation flaps which can be observed as downward spikes in Fig. 11a. In the last week of March and in April, the room temperatures are significantly higher and the upper comfort limit of 24 °C is exceeded in some zones. However, this behavior is limited to three out of the seven zones in Building G, all of which are south-facing. This results in a daily comfort violation of 0.21 Kh/d in March and more than 0.7 Kh/d in April. Similar tendencies of excessive temperatures can also be observed in Buildings A and C, although not as distinctly as in Building G. Reasons for this can be found in the different orientation of the reference zones and the influence of the individual users. As can be observed, the highest zone temperatures often occur and the end of a working day which is a typical behavior of buildings with TABS, see [35] and [36]. Due to internal and external heat gains, the zone temperatures rise during the course of a day and only start to drop again in the evening. Therefore, the lowest temperature that has to be met always occurs at the beginning of a working day.

As described in Section 5.1, there is only very little heating activity in April, indicating that the high room temperatures result mainly from high solar heat gains and partially from internal gains. It is worth to

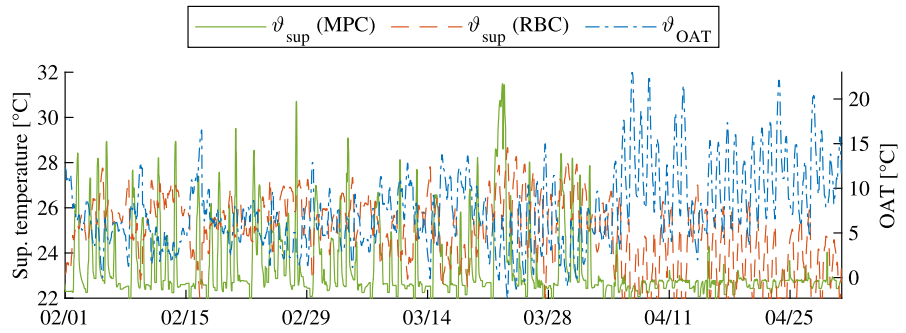

Fig. 9. Comparison of supply temperature set points of the TAC heating circuits generated by MPC and RBC and outside air temperature (OAT).

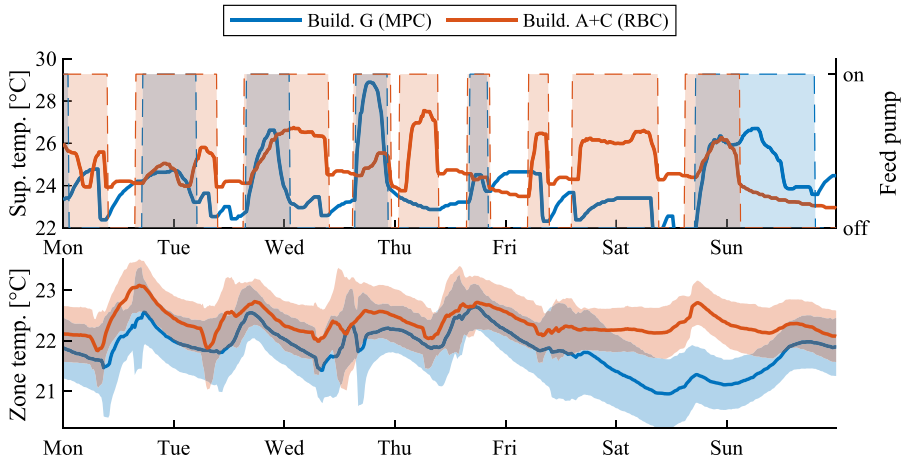

Fig. 10. Resulting supply temperatures from MPC (blue) and RBC (red) with active heating periods (shaded areas) and mean zone temperatures with standard deviation (shaded areas) on the week from 2 to 8 March. (For interpretation of the references to color in this figure legend, the reader is referred to the web version of this article.)

be emphasized that the main challenge of the controller is to meet the lower temperature bound with less heating energy as possible. The violation of the upper temperature bound mainly due to temporary high solar gains is not controllable when slow-reacting TAC are installed, even when MPC is used. Theoretically, cooling via the TAC would have been possible and desirable in April, but due to the default control strategy, the overall system does not switch to cooling mode as this only depends on the OAT (cf. 2.3). This represents the potential for improvement, i. e. by incorporating the operation mode in the MPC algorithm.

The comparison of the comfort violation in the reference offices of the low-rise buildings does not show a clear picture. The MPC operated Building G shows neither a noticeably lower comfort violation nor a significantly higher one compared to Buildings A and C. The thermal comfort is strongly influenced by user behavior, e. g. by using windows or manual shading devices, so that a comfort improvement due to MPC cannot be clearly identified.

To gain a more complete picture of the thermal comfort in the MPC operated building section, additional temperature/humidity data loggers were installed in several offices of different orientations on all five floor levels. Furthermore, the question should be answered as to whether the reference zones on the 4th floor used by the controller are representative of all other offices. In total, 17 data loggers were installed which, together with the seven reference offices, represent about 15% of the offices located in Building G. Fig. 12 shows the average comfort violation per zone in Building G separated by floor. As can be seen, the highest comfort violation occurs in offices on the 1st floor, while the lowest violation can be found on the 3rd floor. There is no standardized value for an acceptable comfort violation in literature. Most studies define a violation of 0.2 Kh to 0.275 Kh per day as tolerable (or 70 Kh to 100 Kh per year). Accordingly, this value is only met on the 3rd and 5th floor, while on all other floors this value is exceeded. Exceeding the upper temperature bound predominates the violation on the 3rd to 5th floor, while on the 1st and 2nd floor violation of the lower bound is dominant. This must be taken into account in the controller design, by carefully choosing comfort bounds which minimize the overall violation. However, due to the topology of the heating system, which does not allow the control of single floors, room for improvement is very limited here. With the exception of the 1st floor, thermal comfort on the other floors is comparable to or better than on the 4th floor. The higher comfort violation on the 4th floor is due to a larger number of south-facing offices included in the investigation compared to the other floors. Even with MPC, the avoidance of temporary temperature peaks as a result of solar heat gains in combination with slow-reacting TAC remains a challenge. Looking at the more important lower temperature bound, controlling the entire building by only taking reference zones on the 4th floor into account is a valid approach.

6. Conclusion

This paper describes the successful implementation of model predictive control in a large-sized office building controlling the supply temperature of a heating circuit for thermoactive ceilings. The MPC makes use of 4th order gray-box models which are implemented in the equation-based modeling language Modelica. Parameters of these models are identified with measurement data from years of operation. The cost function of the controller is a weighted sum of the heating energy demand and the thermal discomfort, resulting in a non-linear optimization problem.

Real operation during a three-month evaluation period from February to April 2020 demonstrated a reduction in heating energy demand of 30% compared to the default rule-based control. Especially

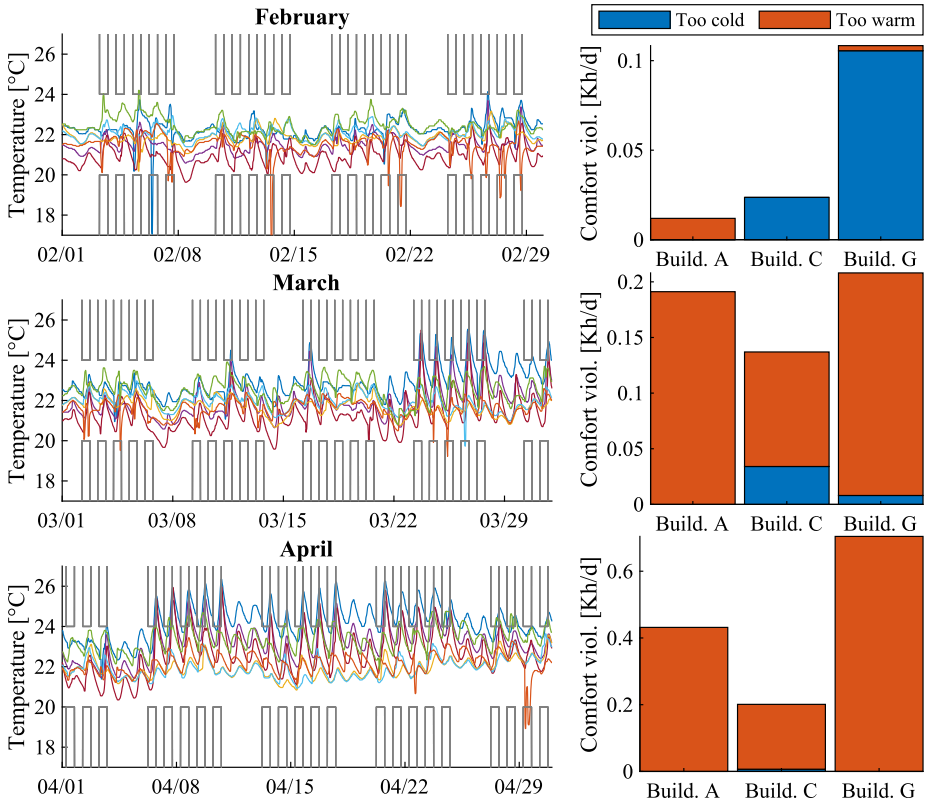

(a) Temperatures of reference zones in Building G.

(b) Average violation of upper and lower comfort bounds per zone and day.

Fig. 11. Experimental results of MPC during the three-month investigation period with regard to thermal comfort.

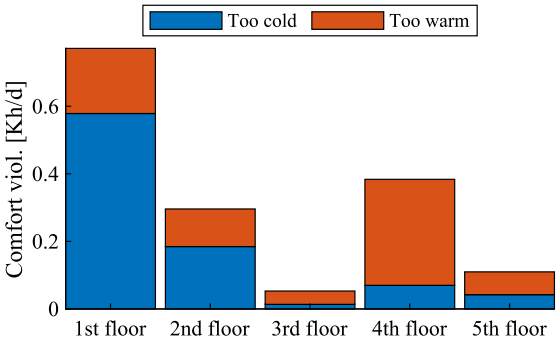

Fig. 12. Average comfort violation per zone and day of Building G in the entire investigation period.

in transition periods like April, characterized by distinct temperature differences between day and night and high solar radiation, the MPC is superior to a heating-curve based control strategy. MPC has once again proven to be a key technology for unlocking the full potential of energy-efficient buildings.

Due to the strong influence of user behavior, an improvement in thermal comfort could not be clearly identified. Further investigations over a longer evaluation period are needed to obtain more reliable results. However, the majority of comfort violations are caused by high temperatures due to solar heat gains. The room for improvement is limited here as a result of restrictions on the heating system and its operation.

Encouraged by the results obtained in this study, the next step is the roll-out of MPC in the entire building. Future work also includes the reduction of modeling effort to obtain building zone models by using adaptive gray-box models, which are identified and tuned automatically during MPC operation. Furthermore, the accuracy of weather and occupancy forecasts can be improved by incorporating on-site measurements to mitigate the disturbance forecast uncertainties.

Nomenclature

Symbols

d	Disturbances
f_{dc}	Discomfort penalty function
f_{occ}	Occupancy penalty function
J_e	Energy cost functions
J_{dc}	Discomfort cost functions
p	Parameters
$\dot{Q}$	Thermal power in W
t	Time in s
t_c	Control horizon in s
T	Temperature in K
u	System input
x	System state
y	System output
α	Weighting factor energy costs
β	Weighting factor discomfort costs
γ	Penalty factor
Δ	Difference
ϑ	Temperature in °C

Abbreviations

AHU	Air-handling unit
BMS	Building management system
EnOB	Energy-optimized building

GHI	Global horizontal irradiance
HDD	Heating degree days
HED	Heating energy demand
LTA	Long-term average
MAT	Monthly average outside air temperature
MPC	Model predictive control
MV	Mechanical ventilation
NLP	Non-linear program
OAT	Outside air temperature
QP	Quadratic program
RBC	Rule-based control
TABS	Thermally activated building system
TAC	Thermoactive ceiling
UKF	Unscented Kalman filter
Indices	
0	Initial value
max	Maximum value
min	Minimum value
occ	Occupancy

Declaration of competing interest

The authors declare that they have no known competing financial interests or personal relationships that could have appeared to influence the work reported in this paper.

References

[1] European Commission, EU transport in figures: Statistical pocketbook 2019, in: EU Transport in Figures, vol. 2019, Publications Office of the European Union, Luxembourg, 2019.

[2] S. Treado, Y. Chen, Saving building energy through advanced control strategies, Energies 6 (9) (2013) 4769–4785.

[3] E. Himpe, M. Vercautere, W. Boydens, L. Helsen, J. Laverge, GEOTABS concept and design: state-of-the-art, challenges and solutions, in: REHVA Annual Meeting Conference Low Carbon Technologies in HVAC, 2018.

[4] G. Serale, M. Fiorentini, A. Capozzoli, D. Bernardini, A. Bemporad, Model predictive control (MPC) for enhancing building and HVAC system energy efficiency: Problem formulation, applications and opportunities, Energies 11 (3) (2018).

[5] M. Sofos, J. Langevin, M. Deru, E. Gupta, K.S. Benne, D. Blum, T. Bohn, R. Fares, N. Fernandez, G. Fink, S. Frank, J. Gerbi, J. Granderson, D. Hoffmeyer, T. Hong, A. Jiron, S. Johnson, S. Katipamula, T. Kuruganti, W.C. Livingood, R. Muehleisen, M. Neukomm, V. Nubbe, P. Phelan, M. Piette, J. Reyna, A. Roth, A. Satre-Meloy, M. Specian, D. Vrabie, M. Wetter, S. Widergren, Innovations in sensors and controls for building energy management: Research and development opportunities report for emerging technologies, 2020.

[6] M. Killian, M. Kozek, Ten questions concerning model predictive control for energy efficient buildings, Build. Environ. 105 (2016) 403–412.

[7] H. Thieblemont, F. Haghighat, R. Ooka, A. Moreau, Predictive control strategies based on weather forecast in buildings with energy storage system: A review of the state-of-the art, Energy Build. 153 (2017) 485–500.

[8] J. Široký, F. Oldewurtel, J. Cigler, S. Prívara, Experimental analysis of model predictive control for an energy efficient building heating system, Appl. Energy 88 (9) (2011) 3079–3087.

[9] S. Prívara, J. Široký, L. Ferkl, J. Cigler, Model predictive control of a building heating system: The first experience, Energy Build. 43 (2–3) (2011) 564–572.

[10] D. Sturzenegger, D. Gyalistras, M. Morari, R.S. Smith, Model predictive climate control of a swiss office building: Implementation, results, and cost–benefit analysis, IEEE Trans. Control Syst. Technol. 24 (1) (2016) 1–12.

[11] R. de Coninck, L. Helsen, Practical implementation and evaluation of model predictive control for an office building in Brussels, Energy Build. 111 (2016) 290–298.

[12] J. Drgoňa, D. Picard, L. Helsen, Cloud-based implementation of white-box model predictive control for a GEOTABS office building: A field test demonstration, J. Process Control 88 (2020) 63–77.

[13] H.T. Haider, O.H. See, W. Elmenreich, A review of residential demand response of smart grid, Renew. Sustain. Energy Rev. 59 (2016) 166–178.

[14] A. Di Giorgio, F. Liberati, Near real time load shifting control for residential electricity prosumers under designed and market indexed pricing models, Appl. Energy 128 (2014) 119–132.

[15] X. Pang, C. Duarte, P. Haves, F. Chuang, Testing and demonstration of model predictive control applied to a radiant slab cooling system in a building test facility, Energy Build. 172 (2018) 432–441.

[16] N. Lazic, C. Boutilier, T. Lu, E. Wong, B. Roy, M. Ryu, G. Imwalle, Data center cooling using model-predictive control, in: Advances in Neural Information Processing Systems, 2018, pp. 3814–3823.

[17] C. Gehbauer, D.H. Blum, T. Wang, E.S. Lee, An assessment of the load modifying potential of model predictive controlled dynamic facades within the California context, Energy Build. 210 (2020).

[18] The Modelica Association, Modelica, 2020.

[19] M. Wetter, M. Bonvini, T.S. Nouidui, Equation-based languages – a new paradigm for building energy modeling, simulation and optimization, Energy and Buildings 117 (2016) 290–300.

[20] P. Niemann, G. Schmitz, Impacts of occupancy on energy demand and thermal comfort for a large-sized administration building, Build. Environ. 182 (2020).

[21] D.H. Blum, K. Arendt, L. Rivalin, M.A. Piette, M. Wetter, C.T. Veje, Practical factors of envelope model setup and their effects on the performance of model predictive control for building heating, ventilating, and air conditioning systems, Appl. Energy 236 (2019) 410–425.

[22] M. Koschenz, B. Lehman, Thermoaktive Bauteilsysteme tabs, 1st edn., EMPA Energiesysteme/Haustechnik, Dübendorf, 2000.

[23] M. Sourbron, Dynamic thermal behaviour of buildings with concrete core activation (Disseration), Katholieke Universiteit Leuven, Leuven, 2012.

[24] Calculation of transient thermal response of rooms and buildings: Modelling of rooms, 2015.

[25] S. Freund, G. Schmitz, Development of a Framework for Model Predictive Control (MPC) in a Large-Sized Office Building Using Modelica Grey-Box Models, in: Proceedings of Building Simulation 2019: 16th Conference of IBPSA, 2019, pp. 2864–2871.

[26] S. Freund, G. Schmitz, Entwicklung und Validierung von Grey-Box-Modellen zur Modellierung des thermischen Verhaltens von Einzelbüros in einem Niedrigenergie-Bürogebäude, in: Proceedings of the BauSIM 2020 - 8th Conference of IBPSA Germany and Austria, 2020, pp. 468–475.

[27] German Weather Services, Model output statistics-MIX (MOSMIX), 2020, https://www.dwd.de/EN/ourservices/met_application_mosmix/met_application_mosmix.html.

[28] Trend Control Systems Limited, 963 supervisor data sheet TA200636 issue 22, 2019, https://partners.trendcontrols.com/trendproducts/cd/en/pdf/en-ta200636-uk0yr0119v.pdf.

[29] MathWorks, OPC toolbox user's guide, 2020, https://de.mathworks.com/help/pdf_doc/opc/opc.pdf.

[30] J. Åkesson, Optimica—an extension of modelica supporting dynamic optimization, in: In 6th International Modelica Conference, 2008, pp. 57–66.

[31] A. Pfeiffer, Optimization library for interactive multi-criteria optimization tasks, in: M. Otter, D. Zimmer (Eds.), Proceedings of the 9th International Modelica Conference, in: Linköping electronic conference proceedings (Online), Linköping University Electronic Press, Linköping, 2012, pp. 669–679.

[32] German Weather Service, Climate data center, observations Germany, climate., 2020, https://opendata.dwd.de/climate_environment/CDC/.

[33] VDI 3807, Characteristic consumption values for buildings: Fundamentals, Beuth Verlag, Berlin, 2013.

[34] DIN EN 15251, Indoor environmental input parameters for design and assessment of energy performance of buildings addressing indoor air quality, thermal environment, lighting and acoustics, Beuth Verlag, Berlin, 2012.

[35] M. Gwerder, B. Lehmann, J. Tödtli, V. Dorer, F. Renggli, Control of thermally-activated building systems (TABS), Appl. Energy 85 (7) (2008) 565–581.

[36] J. Tödtli, M. Gwerder, B. Lehmann, F. Renggli, V. Dorer, TABS Control: Steuerung und Regelung von thermoaktiven Bauteilsystemen; Handbuch für Planung, Faktor Verlag AG, 2009, p. 190.